PCCP

Dynamic Article Links

Cite this: DOI: 10.1039/c0cp02921a

www.rsc.org/pccp

PAPER

Development of a semiempirical potential for simulations of thiol–gold interfaces. Application to thiol-protected gold nanoparticles†

Jimena A. Olmos-Asar,[a] Arnaldo Rapallo[b] and Marcelo M. Mariscal*[a]

Received 20th December 2010, Accepted 3rd February 2011
DOI: 10.1039/c0cp02921a

A new semiempirical potential, based on density functional calculations and a bond-order Morse-like potential, is developed to simulate the adsorption behavior of thiolate molecules on non-planar gold surfaces, including relaxing effects, in a more realistic way. The potential functions include as variables the metal–molecule separation, vibrational frequencies, bending and torsion angles between several pairs of atom types and the coordination number of both the metal (Au) and thiolate groups. The potential was parameterized based on a set of density functional calculations of molecular adsorption in several surface sites (*i.e*. *hollow*, *bridge*, *top*, *on-top* Au adatom and the novel *staple motif*) for different crystalline facets, *i.e*. Au(111) and (100). Langevin dynamics simulations have been performed to study the capping effects of alkanethiolates molecules on Au nanoparticles in the range 1–4 nm. The simulation results reveal an enhancement of the coverage degree whilst the nanoparticles diameter decreases. A high surface disorder due to the strong S–Au bond was found, in very good agreement with very recent experimental findings [M. M. Mariscal, J. A. Olmos-Asar, C. Gutierrez-Wing, A. Mayoral and M. J. Yacaman, *Phys. Chem. Chem. Phys*., 2010, **12**, 11785].

Introduction

The imminent use of metal nanoparticles (NPs) in biomedicine appears as one of the hottest topics in nanoscience. For instance, in recent years DNA–nanoparticles conjugates have been used to build a variety of materials with novel properties.[1,2] Very recently, Au nanoparticles have been used for rapid and sensitive direct detection of *M. tuberculosis* in clinical samples with high efficiency[3] and have been also used for detection of specific DNA and RNA sequences.[4–6]

It is well established now that the Au nanoparticle surface has a strong binding affinity towards thiols.[7] In particular, the thiol–Au interface allows the surface conjugation of various peptides, proteins, and DNA, either *via* a naturally available thiol group such as cysteine[8] or a synthetically incorporated thiol group as in the case of thiolated single-stranded DNA.[4] Therefore, understanding the thiol–Au interface is of crucial importance for future nanotechnology.

In the simplest case, preparation, conservation and protection of metallic nanoparticles require passivation with organic ligand molecules in order to prevent aggregation of the metallic particles. Monolayers self-assembly have been intensively studied, at experimental[9,10] and theoretical levels,[11–14] on extended gold (111) surfaces. Nevertheless, a clear understanding about some fundamental structural aspects of passivated Au nanoparticles still does not exist. In recent times, a great progress in understanding the structure of the thiol/gold interface has been made due to the experimental work of Kornberg and co-workers,[15] which also has motivated a reconsideration of the planar thiol–Au(111) molecular junction.[16]

From a theoretical point of view, calculations can be divided by the level of theory in quantum-mechanics based methods (*i.e*. DFT, Hartree-Fock/HF, Density Functional Tight Binding/DFTB, *etc*.) and semiempirical approaches, where the electronic description is assumed in a specific functional form.

Concerning the first group, most of the studies, reported during the last ten years, are investigations of the interface CH_3S/Au(111) in which intermolecular van der Waals interactions are estimated to be negligible.[17–21] Until 2007, a great controversy about the S–Au(111) interface was installed. Essentially, two singular models were under discussion, *i.e*. adsorption of the thiol head group between a three-fold *hollow* site and a two-fold *bridge* site. Very recently, the consideration of a new adsorption scenario has been introduced. It has been proposed that adsorption of thiolate species with the S group atop Au adatoms is energetically favorable against the

[a] *INFIQC/CONICET, Departamento de Matemática y Física, Facultad de Ciencias Químicas, Universidad Nacional de Córdoba (XUA5000), Córdoba, Argentina. E-mail: marcelo.mariscal@conicet.gov.ar*
[b] *ISMAC-Istituto per lo Studio delle Macromolecole del CNR, via E. Bassini 15, 20133 Milano, Italy*

† Electronic supplementary information (ESI) available: S1: potential energy functions used for intra and intermolecular interactions. S2: diagram of a nanoparticle and radius that defines it. See DOI: 10.1039/c0cp02921a

three-fold or two-fold sites,[21] even more, Au-adatom–dithiolate[22] structural motifs, forming polymer-like structures, appear as the most stable configuration[23] from an energetic point of view.

Regarding the semiempirical approaches, it is interesting to mention the pioneer work performed by Luedtke and Landman[24] where the structure, dynamics, and thermodynamics of gold nanocrystallites passivated by alkylthiolate monolayers were investigated by means of molecular dynamics simulations. However, in such studies the Au atoms were kept fixed during the whole dynamics simulation. Therefore structural information of the gold nanoparticles was unavailable, a very important task to understand the properties and structures of capped nanoparticles. Only, very recently Zachariah and coworkers[25] have reported a molecular dynamics study of an all-mobile-atom approach to study the mechanochemical stability of thiol protected Au NPs. In their work, they reported that the surface of gold nanoparticles becomes highly corrugated by the adsorption of thiol molecules. However, the interatomic potential used to describe the S–Au interface fails to represent the bond-order dependence of the S–Au bond, due that they used a pairwise Morse potential, parameterized to reproduce the adsorption energy of thiols on Au(111) perfect flat surfaces. Therefore, any other local environment is not considered during the parameterization procedure.

Despite the large amount of data available, the exact nature of the bonding between the molecules and the surface is not completely determined and semiempirical approaches to describe the complex energy landscape of the S–Au interface do not exist.

It is well known that the S–Au bond has a large covalent character[26] *i.e.*, chemisorption exists, and the bond is really complex for being correctly described. Theoretical calculations using *ab initio* methods show that the energy, as well as the adsorption site of alkanethiols on metallic substrates depends on the coordination number of the thiolate groups and the coordination of Au atoms. In summary, to accurately describe the S–Au bond, the bond-order (BO) must be taken into account within a functional form of the potential energy.

To the best of our knowledge, at the present, three types of empirical interatomic potentials to describe the S–Au interface are found in the literature. The first are pairwise potentials (Morse and 12–3), fitted to reproduce alkanethiol adsorption on perfect, smooth, immobile Au(111) surfaces.[27] The second, rough surfaces described through a periodic function.[28] And the third type are Morse-like potentials with variable energy parameter well depth, D_e, which varies according to the height of the Au and/or S atoms above the planar surface.[29]

In the present work, we have developed a new semiempirical interatomic potential which, in principle, could be applied to any metal–molecule interface if the potential parameters are known. In the present parameterization we show the case for the S–Au bond which is able to describe interacting species with bond order dependence. The potential has been parameterized using DFT/GGA calculations and subsequently validated, comparing the results with available experiments and *ab initio* calculations. Finally, applications to large thiol-capped gold nanoparticles in the range 1–4 nm (*ca.* 5000 atoms) are presented, sizes unreachable using first-principle calculations at present days.

Simulation method

As mentioned above, aside density functional calculations, most of the computer simulations performed to study the adsorption of alkanethiols on gold surfaces have been tackled using the simple pairwise Morse potential[25,27] or the Hautman–Klein (12–3) potential.[30–32] Nevertheless, these potentials cannot describe in an accurate way the adsorption behavior of these molecules on other interesting systems, like (100) crystalline facets or surface defects, and especially those of low dimensionality, like gold nanowires or nanoparticles. For example, it was recently found that adsorption of thiolates on gold adatoms is energetically more stable than adsorption on flat surfaces.[33,34] But the simple pairwise Morse potential predicts a low adsorption energy on this site (on-top Au adatom), because bond order of sulfur is one ($BO_S = 1$), as in an on-top perfect surface site.

Our aim was to generate a modified Morse potential to represent the covalent interaction between sulfur and gold atoms. In the present formulation, the main characteristic is the existence of variable parameters of the Morse potential that depend on the bond order of both the sulfur and the closest gold atom. This was undertaken by introducing a bond-order, n_j, dependent on the D_e and r_e parameters of the Morse function. The first one takes into account the binding energy and the second one the equilibrium bond distance. The potential function can be described by the following functional form:

$$V_{S-Au}(r,n_{S,Au}) = D_e(n_{S,Au})\exp[-\alpha(r - r_e(n_{S,Au}))] \{\exp[-\alpha(r - r_e(n_{S,Au}))] - 2\} \quad (1)$$

where $D_e(n_{S,Au})$, α, and $r_e(n_{S,Au})$ are fitted parameters and the bond-order is calculated as follows:

$$n_j = \sum_{i \neq j} f(r_{ij}) \quad (2a)$$

$$f(r) = \begin{cases} 1 & r \leq C_1 \\ \frac{1}{2} - \frac{15}{16}\left[Y(r) - \frac{2}{3}Y(r)^3 + \frac{1}{5}Y(r)^5\right] & C_1 < r < C_2 \\ 0 & r \geq C_2 \end{cases} \quad (2b)$$

where

$$Y(r) = \frac{2r - C_2 - C_1}{C_2 - C_1} \quad (2c)$$

and we have taken $C_1 = 2.75$ Å and $C_2 = 3.45$ Å, in order to obtain a smooth slope in the $f(r)$ function, but maintaining all configurations used for the fitting procedure with well-defined bond order values. For calculating Au atoms bond order, we used the same functions, but taking $C_1 = 2.90$ Å and $C_2 = 4.06$ Å. Fig. 1 shows a plot of function $f(r)$.

Six adsorption sites on different substrates were considered during the fitting procedure: two mono-coordinated sites (*on-top* in a perfect (111) flat surface and on a Au adatom),

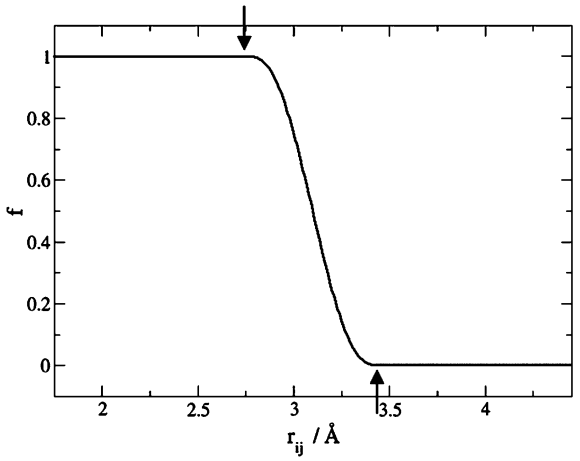

Fig. 1 $f(r)$ function behavior. Arrows indicate C_1 and C_2 cutoffs.

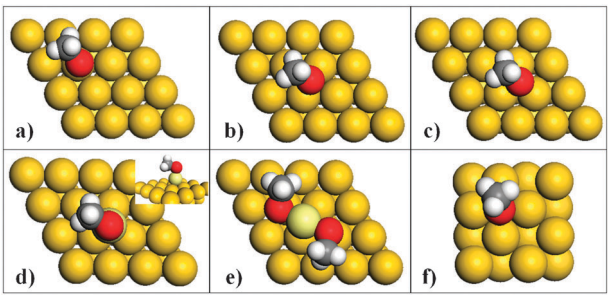

Fig. 2 Adsorption sites considered for the fitting procedure: (a) on-top (b) bridge (c) hollow (111) (d) on-top adatom—inset: lateral view—(e) staple motif "RS–Au–SR" and (f) hollow (100) (color online: red spheres, thiolate group; golden spheres, Au atoms).

one bi-coordinated site (the *bridge* position on a perfect (111) surface), one tri-coordinated site (the *hollow* position in a (111) surface), a tetra-coordinated site (the *hollow* position in a perfect (100) surface) and the staple motif (RS–Au–SR). The six configurations taken into account during the parameterization procedure are shown in Fig. 2.

The adsorption energies (E_{Ad}) for the different sites shown in Fig. 2 were computed using DFT/GGA within the effective core potential approach and double ζ-polarization basis set using the DMOL3 code,[35] according to:

$$E_{Ad} = E_{Au\text{–}SR} - E_{Au} - E_{SR} \quad (3)$$

where the first term represents the total energy of the whole system and the last two, the total energy of the bare Au surface and the isolated molecule respectively.

Table 1 Selected configurations for the potential parameterization, the corresponding adsorption energies in eV and the involved atoms bond orders (BO) for both S and Au

Adsorption site	E_{Ad}/eV	BO (S)	BO (Au)
On-top Au(111)	−1.14	1.00	9.00
Bridge Au(111)	−1.15	2.07	9.00
Hollow Au(111)	−1.17	3.00	9.00
Hollow-bridge Au(111)	−1.34	2.65	9.00
Hollow Au(100)	−2.19	3.98	8.00
Top/adatom-Au(111)	−2.17	1.00	3.00
Motif (RS–Au–SR)/SR group	−2.22	2.00	2.00

Table 2 Optimized values of the parameter D_e in the six selected configurations

Adsorption site	D_e/eV
On-top (111)	0.404764
Bridge (111)	0.271479
Hollow (111)	0.286784
Hollow (100)	0.293681
Top/adatom Au (111)	1.759618
Motif (RS–Au–SR)/SR group	0.782176

The chosen configurations together with E_{Ad} and the bond order number are shown in Table 1.

In each selected configuration, with the molecule adsorbed in its equilibrium position (it implies the S–Au distance at the r_e value), the parameter D_e was changed self-consistently, keeping α as a constant, to reproduce the adsorption energy predicted by DFT calculations. Calculated values are shown in Table 2.

Having these parameters, cubic splines interpolations of the form:

$$D_e = D_e^a\left[2\left(\frac{n-n_a}{n_b-n_a}\right)^3 - 3\left(\frac{n-n_a}{n_b-n_a}\right)^2 + 1\right] + D_e^b\left[3\left(\frac{n-n_a}{n_b-n_a}\right)^2 - 2\left(\frac{n-n_a}{n_b-n_a}\right)^3\right] \quad (4)$$

were performed to obtain values at intermediate positions while satisfying the continuity of the potential energy

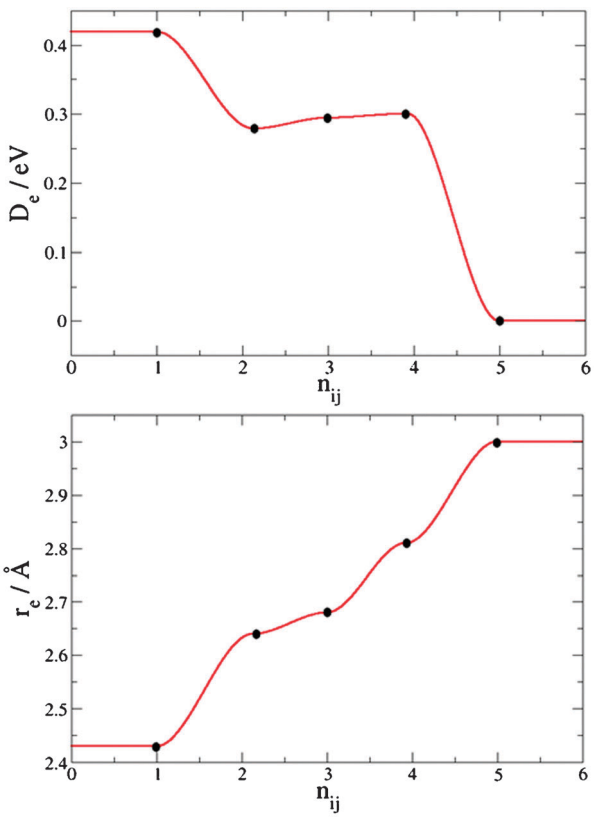

Fig. 3 D_e and r_e parameters as a function of the coordination number. Circles denote the values obtained for each configuration used for the fitting procedure. All other values are taken from cubic splines interpolations.

landscape (D_e^a, D_e^b are the minimum (a) and maximum (b) values of the potential depth at the limits a and b of each interval and n_a, n_b are the BOs at those points). For the r_e parameter, we followed the same procedure to obtain intermediate values. Fig. 3 shows these cubic splines interpolations.

To ensure continuity of the potential in the cutoff, the modified Morse function is splined at long distances according to:

$$V = V_{S\text{–}Au} f_c$$

$$f_c = \frac{1}{2} + \frac{1}{2}\cos\left[\pi \frac{r - r_{min}}{r_{max} - r_{min}}\right] \quad (5)$$

where $r_{min} = C_2$ and $r_{max} = 1$ nm are minimum and maximum distances applied to the cutoff function.

Fig. 4 shows the fitted potential functions for the six configurations mentioned above. The adsorption on the staple motif is the most favorable site, followed by the adsorption onto the on-top a Au adatom, in good accordance with previous density functional calculations.[21,23,36] Note that in the case of the staple motif the well depth corresponds to each S–Au interaction.

The adsorption energy calculated with our potential for the staple motif is −2.21 eV per RS, in good agreement with the *ab initio* calculations reported by Jiang *et al.*[37] of −2.22 eV per RS and considerably more favorable than the "standard" fcc-bridge site (−1.34 eV per SR).

The Au–Au interactions were modeled using the second-moment approximation of the tight binding theory (TB-SMA) which takes into account the many-body character of the metallic bond and has been probed to reproduce most of the characteristic properties of gold. A detailed description of the method can be found in the original work of Cleri and Rosato.[38] In the TB-SMA method, the total energy can be written as the addition of two terms:

$$V = \sum_i \left(\sum_j A_{\alpha\beta} \exp^{-p\alpha\beta\left(\frac{n_j}{r_0^{\alpha\beta}} - 1\right)} - \left\{ \sum_j \xi_{\alpha\beta}^2 \exp^{-2q\alpha\beta\left(\frac{n_j}{r_0^{\alpha\beta}} - 1\right)} \right\}^{-\frac{1}{2}} \right) \quad (6)$$

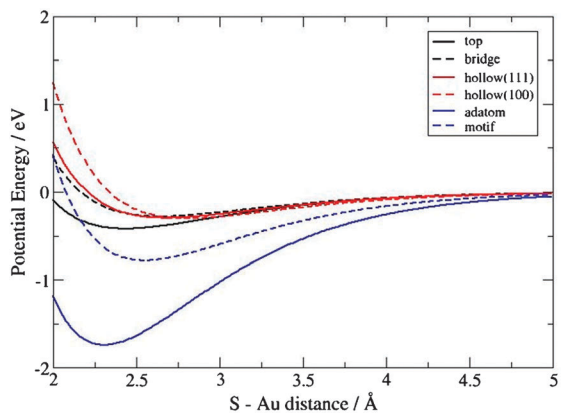

Fig. 4 Fitted potential functions for the S–Au bond for the six configurations taken into account during the parameterization (color online).

Table 3 Values of the potential parameters. k_r is in units of eV Å^{-2}, r_0 in Å, k_θ in eV rad^{-2}, θ_0 in rad, a_n in eV, ε in eV and σ in Å

Interaction	Interacting atoms	Parameter values
Stretching[40]	C–C	$k_r = 30.375$, $r_0 = 1.53$
	C–S	$k_r = 35.625$, $r_0 = 1.82$
Bending[11]	C–C–C	$k_\theta = 5.3931$, $\theta_0 = 1.911$
	C–C–S	$k_\theta = 5.3931$, $\theta_0 = 1.997$
Torsion[11]	C–C–C–C	$a_0 = 9.6199 \times 10^{-2}$
		$a_1 = 1.2602 \times 10^{-1}$
		$a_2 = -1.3602 \times 10^{-1}$
		$a_3 = -3.1722 \times 10^{-2}$
	C–C–C–S	$a_4 = 2.7205 \times 10^{-1}$
		$a_5 = -3.2653 \times 10^{-1}$
van der Waals interactions[11,41]	C–C	$\varepsilon = 5.12 \times 10^{-3}$, $\sigma = 3.905$
	C–S	$\varepsilon = 9.40 \times 10^{-3}$, $\sigma = 4.078$
	S–S	$\varepsilon = 1.72 \times 10^{-2}$, $\sigma = 4.250$
	C–Au	$\varepsilon = 2.77 \times 10^{-3}$, $\sigma = 3.561$

where the first one represents a pair-wise repulsive term and the second one, the band energy, which takes into account the many-body character of the metallic bond.

The intra and inter-molecular interactions of thiolate molecules were represented using the united atom approach by means of the Universal Force Field (UFF)[39] (see ESI† for potential functions). Parameters used in the present simulations are shown in Table 3.

Results

To test the ability of the new potential, we have explored some characteristics of the alkylthiolate/Au interface. For instance, we have computed the adsorption energy of a dodecanethiolate molecule on an unreconstructed Au(111) surface as well as the high coverage structure (*i.e.*$\theta = 0.33$ ML). We have also explored the low-coordination structures and the results are presented in Table 4.

As can be observed, a very good agreement is found with *ab initio* calculations and experimental evidence regarding the structure and the coverage degree.

The atomic configuration of the relaxed structures for $\theta = 0.33$ ML is shown in Fig. 5, where the $\sqrt{3} \times \sqrt{3}(R30^\circ)$ is evident, with 5 Å distance between nearest neighbors. The obtained chain tilt is 34° with respect to the normal of the surface, in very good accordance with previous electronic structure calculations and experimental evidence.[42]

In order to study the effect of thiolate molecules protecting gold nanoparticles, we have performed Langevin dynamics simulations with the purpose of obtaining the dynamic evolution of the adsorption process at a constant temperature, using our own MD/LD code. The computer simulations were conducted as follows:

(a) First, we have performed energy minimizations using the LBFGS quasi-Newtonian nonlinear optimization algorithm and simulated annealing procedures, using a temperature program starting from 100 K, then increasing linearly until 500 K. Finally the temperature is decreased exponentially until it reaches a value of 0.5 K, using a velocity scaling thermostat, to find relaxed structures of the bare gold nanoparticles.

(b) Secondly, an excess of randomly or radially distributed dodecanethiolate species [$CH_3(CH_2)_{11}S$] are built around the

Table 4 Adsorption energy and site found for a low and high-coverage structure of thiolates on a flat unreconstructed perfect Au(111) surface and on a surface with adatoms

System	E_{Ad}/eV (potential)	E_{Ad}/eV (DFT)	Adsorption site
1 CH_3S-unreconstructed Au(111)	−1.46	−1.34	Hollow
1 $CH_3(CH_2)_{11}S$-unreconstructed Au(111)	−1.59	—	Hollow
$\sqrt{3} \times \sqrt{3}(R30°)$-unreconstructed Au(111)	−1.92	−1.83	Hollow
1 CH_3S-unreconstructed Au(111) with adatoms	−2.20	−2.17	On-top (adatom)
CH_3S–Au–CH_3S-unreconstructed Au(111)	−2.22	−2.22	Staple motif

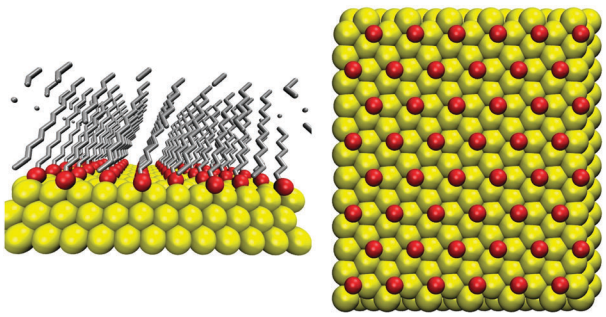

Fig. 5 Adsorption of dodecanethiolate on an unreconstructed Au(111) planar flat surface. The obtained overlayer after simulated annealing, the so-called $\sqrt{3} \times \sqrt{3}(R30°)$ is shown, which corresponds to a $\theta = 0.33$ ML.

relaxed Au NP. Therefore, within this approach, the adsorption sites are not assumed *a priori*. Moreover, concerted diffusion processes are allowed during the dynamics evolution, a key diffusion path, absent in most calculation methods.

(c) Finally, a series of Langevin dynamics simulation have been performed using a timestep of 1 fs during 2 ns in order to mimic the adsorption of the *n*-dodecanethiolate molecules including the effect of the solvent molecules through stochastic and frictional forces.

Fig. 6 shows the maximum coverage degree for nanoparticles of different geometry, *i.e.* cuboctahedra (CO), icosahedra (Ico) and regular decahedra (Dh) for several sizes, starting from Au_{55} to Au_{1419}.

The coverage degree has been defined as the ratio between the number of adsorbed molecules and the initial number of

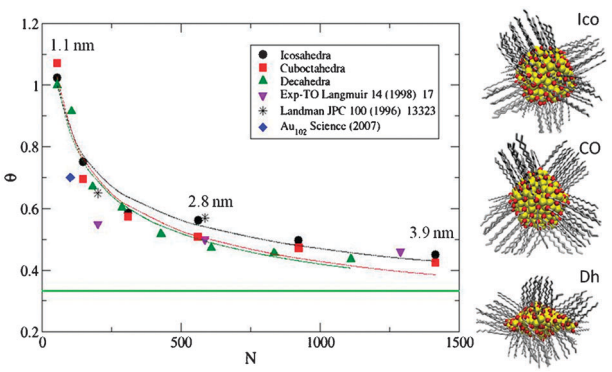

Fig. 6 Left: nanoparticle coverage as a function of *N* (the number of metal atoms in the NP). Black circles: Ico, red squares: CO, green triangles: Dh. Right: atomic configurations of thiol-protected Au NPs (color online).

surface gold atoms in the NP. As can be noted in the figure, the coverage degree increases markedly as the nanoparticle diameter decreases, reaching a limit value close to one when the NP diameter is nearby 1 nm. It is important to note that, when the nanoparticles diameter reaches a value of approximately (1500 atoms), the coverage degree tends to the value of the planar surface, *i.e.* 0.33 ML (marked in Fig. 6 with a solid green line). Note that an experimental estimation[43] of the coverage degree is also plotted, as well the results taken from the early work of Luedtke and Landman[24] and the novel discoveries of Kornberg and co-workers.[15]

Each set of data obtained from the simulations has been fitted using the following function:

$$\theta = A_i N^{-\alpha_i} \quad (7)$$

where the index *i* refers to the nanoparticle geometry, *i.e.* CO, Ico, Dh. The A_i and α_i parameters obtained are shown in Table 5.

In a first analysis, we can explain the difference in the coverage degree on different NP structures as a curvature effect rather than a facet effect. This can be supported by the fact that a high surface disorder is observed after thiol-adsorption, due to the strong S–Au bond, particularly in small nanoparticles.[44] Considering each nanoparticle as a sphere, we can estimate the extrinsic curvature (ξ) by taking the reciprocal of its radius. In Fig. 7 the coverage degree is plotted against the curvature of the nanoparticle. A linear relationship of the form ($\theta = 0.235 + 4.214\xi$) has been obtained, and it is also shown in Fig. 7.

In order to quantify the degree of sphericity of a given nanoparticle we define the factor $\gamma = \frac{rb-ra}{ra}$, where *rb* represents the radius of a sphere containing a nanoparticle with radius *ra* (see ESI†). In this sense, a value of γ equal to zero means that the nanoparticle can be described as a perfect sphere. The calculated values of γ for the three structures are: $\gamma_{ICO} = 0.22$, $\gamma_{CO} = 0.41$ and $\gamma_{Dh} = 1.42$. From these results and taking into account the results shown in Fig. 6 we can summarize that, for a given particle diameter, the coverage degree increases with the sphericity of the nanoparticle.

The bond orders of S atoms were also recorded for the relaxed structures, and plotted in Fig. 8 for the three morphologies considered. As expected, a maximum BO_S close to four was

Table 5 Parameters obtained from fitting equation $\theta = A_i N^{-\alpha_i}$

Geometry	A_i	α_i
Icosahedra	2.835	0.26
Cuboctahedra	3.446	0.30
Decahedra	3.475	0.31

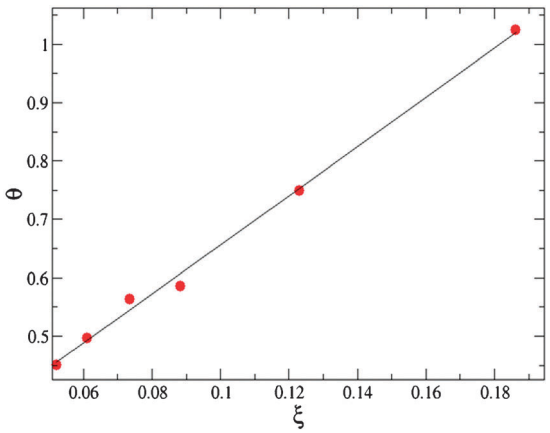

Fig. 7 Coverage degree as a function of the curvature ξ of the nanoparticle for the case of icosahedra structures.

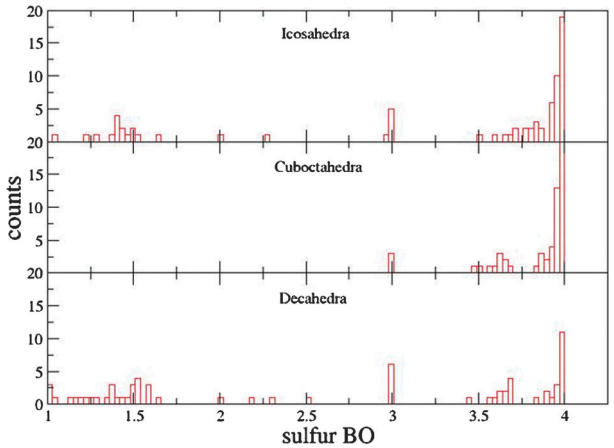

Fig. 8 Bond order distribution of S atoms in three capped Au nanoparticles of different geometries: Ico_{561}, CO_{561} and Dh_{609}.

reached in all cases, corresponding to the adsorption in flat facets. But, a distribution of values near 1.5 was also observed in the case of icosahedra and decahedra geometries, which can be attributed to low-coordination structures as adatoms and staple-motifs. Note that these bond orders are absent in nanoparticles with large {100} facets, *i.e.* cuboctahedral nanoparticles.

Conclusions

In the present work a new semiempirical potential was developed to describe the thiol–Au interface in a more realistic way. The potential functions include as variables the metal–molecule separation, vibration frequencies, bending and torsion angles between several pairs of atom types and the bond order dependence of both the metal (Au) and S atoms. The potential was parameterized based on a set of DFT calculations of molecular adsorption in several surface sites (*i.e.* hollow, bridge, top and on-top an adatom and the novel staple motif). It is interesting to mention that the same methodology could be used for other molecule–metal systems, opening the way to further research.

Langevin dynamics simulations, using the new semi-empirical potential, were performed to explore the coverage degree of Au nanoparticles of several morphologies using dodecanethiol as the capping agent. The studied NPs are in the range 1–4 nm, which at present time is difficult to access with high-level electronic calculations. The results reveal a high enhancement of the coverage degree when the nanoparticle diameter decreases to values near 1–2 nm.

Acknowledgements

The authors wish to thank CONICET and CNR for an International Cooperation program, Secyt UNC, Program BID (PICT 2007 N° 00340), PIP: 112-200801-000983, PME: 2006-01581 and M. J. Yacaman for interesting discussions and financial support. J. A. Olmos-Asar thanks CONICET for the fellowship.

Notes and references

1 A. P. Alivisatos, K. P. Johnsson, X. Peng, T. E. Wilson, C. J. Loweth, M. P. Bruchez Jr. and P. G. Schultz, *Nature*, 1996, **382**, 609.
2 C. J. Loweth, W. B. Caldwell, X. Peng, A. P. Alivisatos and P. G. Schultz, *Angew. Chem., Int. Ed.*, 1999, **38**, 1808.
3 P. V. Baptista, M. Koziol-Montewka, J. Paluch-Oles, G. Doria and R. Franco, *Clin. Chem. (Washington, D. C.)*, 2006, **52**, 1433.
4 C. A. Mirkin, R. L. Letsinger, R. C. Mucic and J. J. Storhoff, *Nature*, 1996, **382**, 607.
5 J. J. Storhoff, R. Elghanian, R. C. Mucic, C. A. Mirkin and R. L. Letsinger, *J. Am. Chem. Soc.*, 1998, **120**, 1959.
6 P. Baptista, G. Doria, D. Henriques, E. Pereira and R. Franco, *J. Biotechnol.*, 2005, **119**, 111.
7 E. Katz and I. Willner, *Angew. Chem., Int. Ed.*, 2004, **43**, 6042.
8 K. Naka, H. Itoh, Y. Tampo and Y. Chujo, *Langmuir*, 2003, **19**, 5546.
9 A. Ulman, S. D. Evans, Y. Shnidman, R. Sharma, E. Eilers and J. C. Chang, *J. Am. Chem. Soc.*, 1991, **113**, 1499.
10 D. J. Lavrich, S. M. Wetterer, S. L. Bernasek and G. Scoles, *J. Phys. Chem. B*, 1998, **102**, 3456.
11 J. Hautman and M. Klein, *J. Chem. Phys.*, 1989, **91**, 4994.
12 A. Pertsin and M. Grunze, *Langmuir*, 1994, **10**, 3668.
13 Y. Yourdshahyan and A. M. Rappe, *J. Chem. Phys.*, 2002, **117**, 825.
14 M. J. Esplandiú, M. L. Carot, F. P. Cometto, V. A. Macagno and E. M. Patrito, *Surf. Sci.*, 2006, **600**, 155.
15 P. D. Jadzinsky, G. Calero, C. J. Ackerson, D. A. Bushnell and R. D. Kornberg, *Science*, 2007, **318**, 430.
16 A. Cossaro, R. Mazzarello, R. Rousseau, L. Casalis, A. Verdini, A. Kohlmeyr, L. Floreano, S. Scandolo, A. Morgante, M. L. Klein and G. Scoles, *Science*, 2008, **321**, 943.
17 H. Grönbeck, A. Curioni and W. Andreoni, *J. Am. Chem. Soc.*, 2006, **122**, 3839.
18 M. Tachibana, K. Yoshizawa, A. Ogawa, H. Fujimoto and R. Hofmann, *J. Phys. Chem. B*, 2002, **106**, 12727.
19 J. Gottschalck and B. Hammer, *J. Chem. Phys.*, 2002, **116**, 784.
20 Y. Morikawa, T. Hayashi, C. C. Liew and H. Nozoye, *Surf. Sci.*, 2002, **46**, 507.
21 F. P. Cometto, P. Paredes-Olivera, V. A. Macagno and E. M. Patrito, *J. Phys. Chem. B*, 2005, **109**, 21737.
22 O. Voznyy, J. J. Dubowski, J. T. Yates Jr. and P. Maksymovych, *J. Am Chem. Soc.*, 2009, **131**, 12989.
23 H. Grönbeck and H. Häkkinen, *J. Phys. Chem. B*, 2007, **111**, 3325.
24 W. D. Luedtke and U. Landman, *J. Phys. Chem.*, 1996, **100**, 13323.
25 B. J. Henz, T. Hawa and M. R. Zachariah, *Langmuir*, 2008, **24**, 773.
26 N. Gonzalez-Lakunza, N. Lorente and A. Arnau, *J. Phys. Chem. C*, 2007, **111**, 12383.
27 R. Mahaffy, R. Bhatia and B. J. Garrison, *J. Phys. Chem. B*, 1997, **101**, 771.
28 B. Jeon, J. D. Kress and N. Grønbech-Jensen, *Phys. Rev. B: Condens. Matter*, 2007, **76**, 155120.
29 K. S. S. Liu, C. W. Yong, B. J. Garrison and J. C. Vickerman, *J. Phys. Chem. B*, 1999, **103**, 3195.

30 J. Hauptman and M. J. Klein, *Chem. Phys*., 1989, **91**, 4994.
31 R. Pool, P. Schapotschnikow and T. J. H. Vlugt, *J. Phys. Chem. C*, 2007, **111**, 10201.
32 O. S. Lee and G. C. Schatz, *J. Phys. Chem. C*, 2009, **113**, 2316.
33 P. Maksymovych, D. C. Sorescu and J. T. Yates, *Phys. Rev. Lett*., 2006, **97**, 146103.
34 A. Bencini, G. Rajaraman, F. Totti and M. Tussa, *Superlattices Microstruct*., 2009, **46**, 4.
35 B. Delley, *J. Chem. Phys*., 2000, **113**, 7756.
36 H. Grönbeck and M. Odelius, *Phys. Rev. B: Condens. Matter*, 2010, **82**, 085416.
37 D. Jiang, M. L. Tiago, W. Luo and S. Dai, *J. Am. Chem. Soc*., 2008, **130**, 2777.
38 F. Cleri and V. Rosato, *Phys. Rev. B: Condens. Matter*, 1993, **48**, 22.
39 A. K. Rappe, C. J. Casewit, K. S. Colwell, W. A. Goddard III and W. M. Skiff, *J. Am. Chem. Soc*., 1992, **114**, 10024.
40 A. W. Rosenbaum, M. A. Freedman, S. B. Darling, I. Popova and S. J. Sibener, *J. Chem. Phys*., 2004, **120**, 3880.
41 K. S. S. Liu, C. W. Yong, B. J. Garrison and J. C. Vickerman, *J. Phys. Chem. B*, 1999, **103**, 3195.
42 C. Vericat, M. E. Vela, G. Benitez, P. Carro and R. C. Salvarezza, *Chem. Soc. Rev*., 2010, **39**, 1805.
43 M. J. Hostetler, J. E. Wingate, C. Jian Zhong, J. E. Harris, R. W. Vachet, M. R. Clark, J. D. Londono, S. J. Green, J. J. Stokes, G. D. Wignall, G. L. Glish, M. D. Porter, N. D. Evans and R. W. Murray, *Langmuir*, 1998, **14**, 17.
44 M. M. Mariscal, J. A. Olmos-Asar, C. Gutierrez-Wing, A. Mayoral and M. J. Yacaman, *Phys. Chem. Chem. Phys*., 2010, **12**, 11785.